16th World Conference on Earthquake, 16WCEE 2017

Santiago Chile, January 9th to 13th 2017

Paper N° 4067

Registration Code: S-L1462965035

AN IMPROVED MACROELEMENT MODEL ACCOUNTING FOR ENERGY DISSIPATION IN IN-PLANE FLEXURAL BEHAVIOUR OF MASONRY WALLS

S. Bracchi[(1)], A. Galasco [(2)], A. Penna [(3)]

[(1)] *PhD Candidate, ROSE Programme, UME School, Institute for Advanced Studies, via Ferrata 1, I-27100 Pavia, Italy, stefano.bracchi@umeschool.it*
[(2)] *Post-doctoral researcher, University of Pavia, Department of Civil Engineering and Architecture via Ferrata 3, I-27100 Pavia, Italy, alessandro.galasco@unipv.it*
[(3)] *Associate Professor, University of Pavia, Department of Civil Engineering and Architecture via Ferrata 3, I-27100 Pavia, Italy, andrea.penna@unipv.it*

Abstract

In the numerical modelling of flexural behaviour of masonry buildings by means of macroelement models, it is important to account for the limited compressive strength and the proper energy dissipation of the material. The macroelement model currently implemented in the TREMURI computer program is featured by a bi-linear compressive behaviour with limited strength, capable of accounting for toe-crushing during cyclic loads, and no tension strength. In addition, in the constitutive relationship, the secant unloading-reloading branch allows for energy dissipation, together with stiffness degradation. From the numerical simulation of experimental tests, an underestimation of the dissipated energy during cyclic loads was noticed. In order to better capture the energy dissipation, in this work an improved model is proposed. In addition to the assumption of limited compressive strength and no tension behaviour, the improved model is characterized by an unloading branch with slope equal to the initial stiffness, thus allowing an increased energy dissipation and the ability of modelling displacement accumulation. The new macroelement model is then implemented in the TREMURI program. In order to validate the model, comparisons with distributed nonlinear spring models implementing the same constitutive relationship and simulations of experimental tests on masonry piers are performed.

Keywords: masonry; macroelement model; nonlinear analysis; energy dissipation

1. Introduction

The high seismic vulnerability of existing masonry buildings, evident from past and recent earthquakes, has led to the necessity of modelling approaches suitable for static and dynamic analysis of both masonry walls and buildings. Different approaches have been proposed in the past, ranging from the micromodelling techniques (e.g. [1]), in which a refined discretization of units, mortar and interfaces by nonlinear finite elements is proposed, to equivalent continuum models (e.g. [2, 3]), in which masonry is idealized as an equivalent homogenized material, derived from the mechanical properties of the components. Discrete and/or rigid element approaches (e.g. [4, 5]) can be considered as alternatives to the previously mentioned finite element models. All these models are characterized by a high computational burden which limits their applicability to simple structures. For this reason, simplified models, based on storey mechanism (e.g. [6]) or limit analysis (e.g. [7]), have been proposed and used, although they can be adopted only under restrictive hypotheses.

A good compromise between accuracy of results and computational burden consists in the so-called macroelement approach (e.g. [8]), usually implemented in an equivalent-frame model of the building. In particular, a single macroelement is used to model the response of a masonry element (pier or spandrel beam). The in-plane behaviour of an entire masonry wall can then be modelled assembling macroelements, using equivalent frame techniques (e.g. [9, 10]). Among these macroelement models, the model proposed in [11] is particularly suitable for the analysis of buildings and it has been implemented in the TREMURI [12] computer program for the nonlinear analysis of masonry buildings. This model includes, in particular, a nonlinear degrading law for rocking damage, which allows to take into account the effect of limited compressive strength (toe-crushing).

The aim of this paper is to propose an improved version of the macroelement model presented in [11] in order to better account for energy dissipation in in-plane flexural failure modes of masonry walls; the model can thus be able to better simulate the experimental cyclic response of masonry panels.

2. Macroelement model of masonry walls

The basic ideas of the 2-node macroelement model proposed in [11] are illustrated in Fig. 1. The panel is ideally subdivided into three parts: a central body, where only shear deformations are possible, and two interfaces, where the external degrees of freedom are located, which can have relative axial displacements and rotations with respect to those of the extremities of the central body. The two interfaces can be considered infinitely rigid in shear and have a negligible thickness. Their axial deformations are due to a system of distributed zero-length springs.

These assumptions simplify the macroelement kinematics and compatibility relations allow to obtain a reduction of the actual degrees of freedom of the model. Since the central part is considered as a rigid body with only shear deformation capability, under small displacement hypotheses, the axial displacements and rotations of the ends can be considered equal to the centroid ones (w_e, φ_e), whereas the transversal displacements of the central body ends must be equal to the corresponding nodal displacements (u_i, u_j). Therefore, the macroelement kinematics can be described by means of eight degrees of freedom, six nodal displacement components (u_i, w_i, φ_i, u_j, w_j, φ_j) and two internal components (w_e, φ_e). No distributed transversal actions are considered and so the internal shear force is constant along the element axis ($V_i = V_j = V$). A no tension model has been attributed to zero-length springs at the interfaces, with a bilinear degrading constitutive model in compression.

The next section describes the axial and flexural behaviour of the improved macroelement model. The shear damage model is not described here since it is equal to the one proposed in [11].

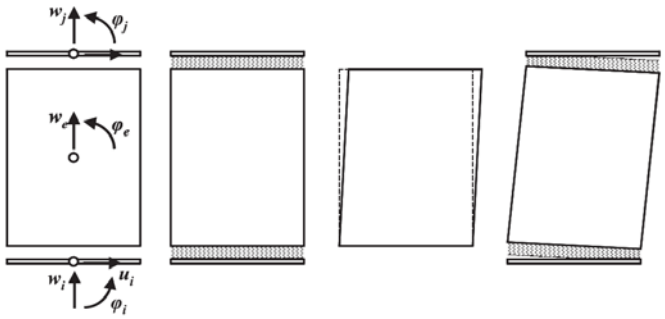

Fig. 1 – Kinematics of the macroelement [1]

3. Improved macroelement model for flexural failure modes

As in the original model [1], the axial and flexural behaviour of the two extremity joints is studied separately. The static and kinematic variables involved in the joint model are the element forces N and M for the considered node and the relative displacement components w and φ. The relations between such variables are directly derived from the constitutive model. In particular, if the whole cross section is compressed, no cracking occurs and the problem is uncoupled, with linear relations linking N and M with w and φ respectively:

$$\begin{cases} N = kltw \\ M = \dfrac{k}{12} tl^3 \varphi \end{cases} \tag{1}$$

where l is the wall length, t is the wall thickness, $k = 2E/h$ is the spring axial stiffness for surface unit, E is the compressive Young modulus of masonry, h is the wall height, w is the relative axial displacement ($w = w_i - w_e$ at node i and $w = w_e - w_j$ at node j) and φ is the relative rotation ($\varphi = \varphi_i - \varphi_e$ at node i and $\varphi = \varphi_e - \varphi_j$ at node j).

The cracking condition can be expressed in terms of kinematic variables (Fig. 2):

$$|\varphi| > \frac{2w}{l} \tag{2}$$

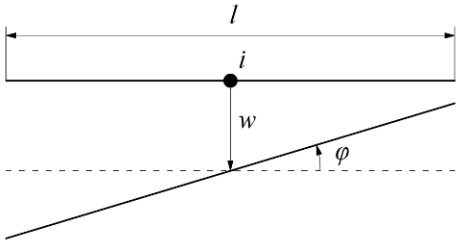

Fig. 2 – Kinematic variables at node i interface [1]

As shown in [11], the axial force and moment, accounting for cracking, can be calculated as the elastic contribution corrected with the contributions due to cracking. For node i interface, these relations can be written in matrix form as:

$$\begin{Bmatrix} N_i \\ M_i \end{Bmatrix} = \begin{bmatrix} ktl & 0 \\ 0 & \dfrac{ktl^3}{12} \end{bmatrix} \begin{Bmatrix} w_i - w_e \\ \varphi_i - \varphi_e \end{Bmatrix} - \begin{Bmatrix} N_i^*(w_i, w_e, \varphi_i, \varphi_e) \\ M_i^*(w_i, w_e, \varphi_i, \varphi_e) \end{Bmatrix} \tag{3}$$

where N_i^* and M_i^* are the inelastic corrections due to cross section cracking and can be calculated as described in [11]. Similar constitutive equations can be derived for the interface joint at node j.

Masonry compressive strength is usually high with respect to the vertical stress due to static vertical loads. Nevertheless, experimental tests (e.g. [13, 14, 15]) showed that in-plane rocking is often characterized by toe-crushing phenomena at the base of masonry piers, causing the limitation of the ultimate bending moment and

some stiffness degradation in the following cycles. In order to include such effects into the nonlinear macroelement model, in [11] a phenomenological bilinear constitutive model with stiffness degradation (illustrated in the left part of Fig. 3) was assigned to the interface joint springs. When the displacement threshold d_y is exceeded, the compressive stress in the springs is limited at the value f_m and the stiffness is degraded to the secant value at the maximum displacement attained during previous load history (d_{max}). Whereas this model provides a good simulation of the experimentally observed strength of masonry walls, it provides a significant underestimation of the energy dissipated during load cycles. Moreover, this model is not able to account for residual displacement and consequently for damage accumulation in previous load history.

In this work, an improved model is introduced, characterized by a limited compressive strength f_m and unloading stiffness equal to the elastic one (illustrated in the right part of Fig. 3). The increased hysteresis of the constitutive law allows an increased energy dissipation; furthermore, this model is able to account for residual displacements after unloading and so it can reproduce damage accumulation due to displacement accumulation during load history. Furthermore, this ability of modelling residual displacements makes the improved model particularly suitable for capturing also the soil crushing during cyclic loads.

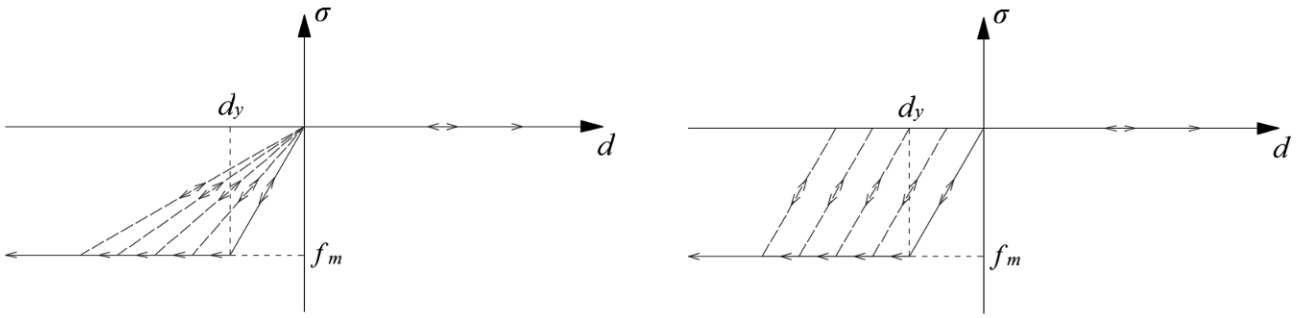

Fig. 3 – Original constitutive model, with no tensile and limited compressive strength and compressive stiffness degradation, for interface joint springs [11] (left) and improved constitutive model, with no tensile and limited compressive strength, residual displacement and increased energy dissipation, for interface joint springs (right)

The local compression displacement ductility can be defined as:

$$\mu = \frac{d_{\max}}{d_y} \tag{4}$$

with $d_y = f_m/k$.

Similarly to what done in [11], the nonlinear correction associated with toe-crushing is performed introducing two damage variables for each cross section edge: the ductility demand in the external compressed spring at the current load step (μ') and the ratio of the length of the portion of the cross section involved in crushing nonlinearity (i.e. the plasticized portion of the section) and the length of the whole section, at the current load step (ζ'). The two variables can be calculated as:

$$\mu' = \frac{d_{\max}}{d_y}; \quad \zeta' = \frac{(\mu' - 1) d_y}{\varphi l} \tag{5}$$

In addition to the values of these two variables at the current load step, also the maximum values of these variables reached during the load history up to the current load step (μ and ζ, respectively) need to be introduced. These variables represent the damage cumulated during previous load history. The nonlinear corrections to N and M depend on all the four crushing damage variables μ, μ', ζ and ζ'.

Fig. 4 shows an example of the displacement and the corresponding vertical stress distributions (thick black lines) in case the load is increased monotonically (e.g. imposing a constant displacement of the centre of the section w and monotonically increasing the rotation φ) until a portion of the section reaches the yield displacement d_y without cracking of the section (case (a)). It can be noticed that, when the displacement exceeds the yield displacement d_y, the vertical stress is constant and equal to the compressive strength f_m. The current

ductility demand μ' and the current normalized length of the plasticized portion ζ' coincide with the maximum values reached during load history (μ and ζ). Furthermore, Fig. 4 shows the displacement and vertical stress distributions (thick black lines) in case, starting from a condition in which crushing of a portion of the section with length ζl was attained, the vertical displacement is maintained fixed and the rotation is reduced, i.e. the displacement of the right edge reduces while remaining positive (i.e. right edge remains compressed). It should be noticed that, when reducing the displacement of the right edge, two different stress distributions can be obtained depending on the amount of reduction of displacement. If the reduction is not sufficient to reach the zero vertical stress, the whole section still remains compressed (case (b)), whereas, if the zero vertical stress is attained in the right edge, the stress profile over the section is characterized by a zone of zero stress (case (c)).

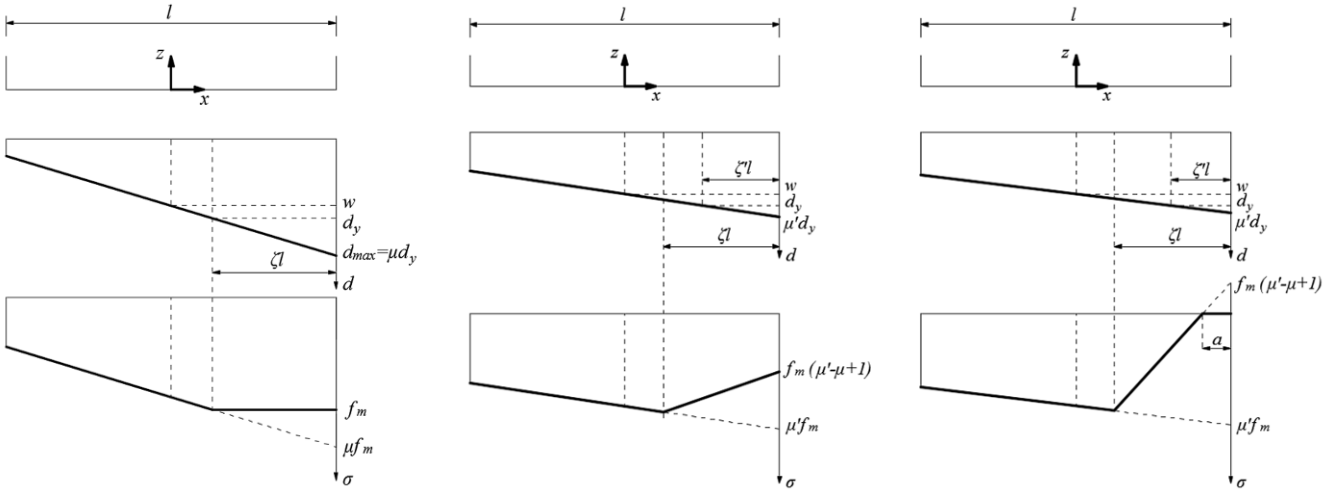

(a) **(b)** **(c)**

Fig. 4 – Displacement and stress distributions along the cross section in case the nonlinear compressive behaviour is activated: loading (a) and unloading in the case the vertical stress at the right edge is greater (b) or equal (c) to zero (no cracking)

In both the cases of loading (case (a)) and unloading with stress different from zero in the whole section (case (b)), the correction factors of N and M accounting for toe-crushing can be obtained simply considering the additional area present in the stress profile when a linear elastic behaviour is assumed with respect to the actual nonlinear stress distribution (multiplying it times the thickness of the section t). In particular, for both the cases (a) and (b), the correction factors N^{**} and M^{**} can be calculated as:

$$N_i^{**} = \frac{1}{2}\Delta\sigma\zeta l t = \frac{1}{2} f_m \zeta l t(\mu - 1)$$
$$M_i^{**} = N_i^{**}\left(\frac{l}{2} - \frac{\zeta l}{3}\right) \tag{6}$$

In the case a portion of the section (of length a) is characterized by zero stress (case (c)), the correction factors are represented by the area of the trapezoid between the elastic stress profile (dashed black line) and the actual one (thick black line). In order to determine this area, the length a characterized by zero stress can be calculated using similitude of triangles. The correction factors N^{**} and M^{**} can be finally obtained as:

$$N_i^{**} = \frac{1}{2} f_m \zeta l t(\mu - 1) - \frac{1}{2} f_m a t(\mu' - \mu + 1)$$
$$M_i^{**} = \frac{1}{2} f_m \zeta l t(\mu - 1)\left(\frac{l}{2} - \frac{\zeta l}{3}\right) - \frac{1}{2} f_m a t(\mu' - \mu + 1)\left(\frac{l}{2} - \frac{a}{3}\right) \tag{7}$$

In a generic load step, the section can be cracked, i.e. the displacement of one edge can be negative. In this case, with reference to the edge where cracking is developing, two situations can be distinguished:

1) the cracked length (l_C) is lower than the plasticized length (ζl), $l_C \leq \zeta l$;
2) the cracked length (l_C) is higher than the plasticized length (ζl), $l_C > \zeta l$.

Fig. 5 shows the displacement and vertical stress distributions (thick black lines) in case the cracked length is lower than the plasticized one. Since both the edges come into play in the nonlinear correction, in order to distinguish the contribution of the two sides, the subscripts *R* and *L*, referring to right and left edge respectively, have been introduced. The correction factors *N*** and *M*** are due to the area indicated by the red shading. The contributions to the correction factors *N*** and *M*** due to the right part of this area can be calculated using Eq. (6) or (7). In order to calculate the contributions due to the left part of the area, the cracked length $l_{C,L}$ has to be calculated as a function of the vertical displacement *w* and the rotation φ.

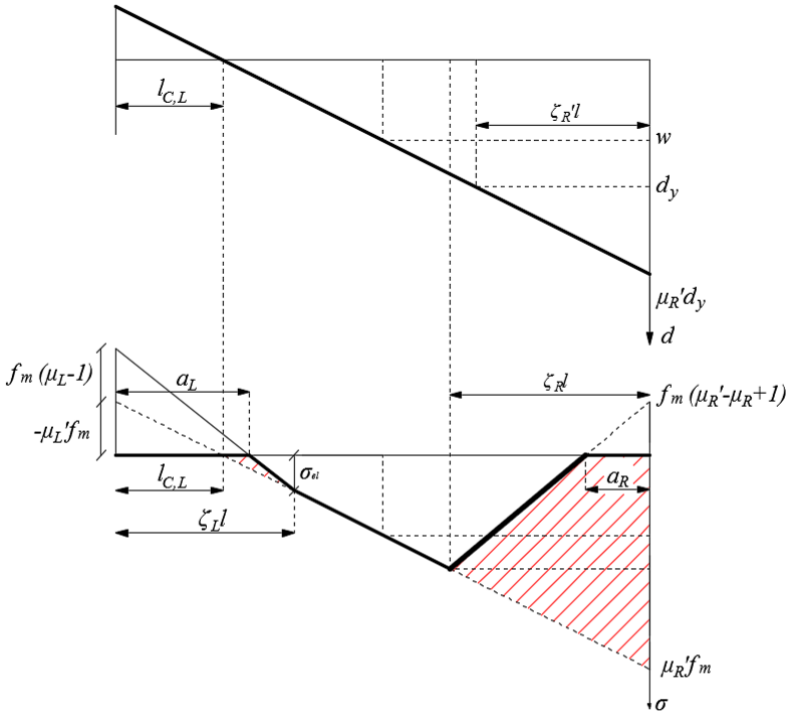

Fig. 5 – Displacement and stress distributions along the cross section in case of nonlinear compressive behaviour with cracked section and cracked length lower than the plasticized length

The length a_L indicated in Fig. 5 can then be obtained using similar triangles, whereas the correction factors *N*** due to the left area can be obtained as summation/subtraction of areas of triangles:

$$N_i^{**} = \frac{1}{2} f_m \zeta_L l t (\mu_L - 1) - \frac{1}{2} f_m a_L t (\mu_L - 1 - \mu_L') - \frac{1}{2} \mu_L' f_m l_{C,L} t \tag{8}$$

Similarly, the correction factors *M*** due to the left area is obtained as the product of *N*** times the corresponding eccentricity e_L:

$$M_i^{**} = N_i^{**} e_L \tag{9}$$

In the case the length of the cracked zone is greater than the plasticized length, the correction factors *N*** and *M*** are only due to the right part of the shaded area of Fig. 5 and they can be obtained using Eq. (6) or (7).

Finally, the values of N and M accounting for nonlinearities due to both cracking and toe-crushing can be obtained as:

$$N_i = ktlw - N_i^* - N_i^{**}$$
$$M_i = \frac{1}{12} ktl^3 \varphi - M_i^* - M_i^{**} \quad (10)$$

where N_i^* and M_i^* are the correction factors due to cracking and N_i^{**} and M_i^{**} are the correction factors due to toe-crushing. The same procedure is obviously valid also for node j.

At each load step, the current values of each of the two damage variables at each corner of the macroelement can be lower or greater than the maximum values. When the current value is greater than the maximum one, the corresponding damage variable has to be updated, because a new condition of nonlinearity has been attained. Finally, the improved macroelement model was implemented in the TREMURI computer program [12] for the nonlinear analysis of masonry buildings.

After the theoretical development of the improved macroelement, the responses obtained by means of the current and the improved model were compared. In order to do this, a calcium-silicate wall of length 2 m, height 4.4 m and thickness 0.1 m with double fixed static scheme was considered. The material properties were assumed equal to the ones determined in the first phase of an experimental campaign recently performed at EUCENTRE in Pavia (Italy) on calcium-silicate brick walls [17]: in particular, the elastic modulus and the compressive strength are equal to 2300 MPa and 5.6 MPa respectively. The wall is subjected to an imposed constant axial load (500 kN) and an increasing cyclic horizontal top displacement up to a value of 0.018 m. Fig. 6 shows the vertical displacement of the top of the wall (left) and the moment (right) versus the macroelement rotation, obtained by means of the current (black lines) and the improved (red lines) macroelement model. By comparing the moment obtained by means of the two models, it is evident how the improved model allows an increased energy dissipation maintaining the same strength. By looking at the vertical displacement, it can be noticed that the accumulation of vertical displacement is higher with the improved model, meaning that the improved model is able of better capturing damage accumulation; if the simulation had been performed at constant vertical displacement, this would have resulted in a higher reduction of axial load with the increase of rotation with respect to the current model.

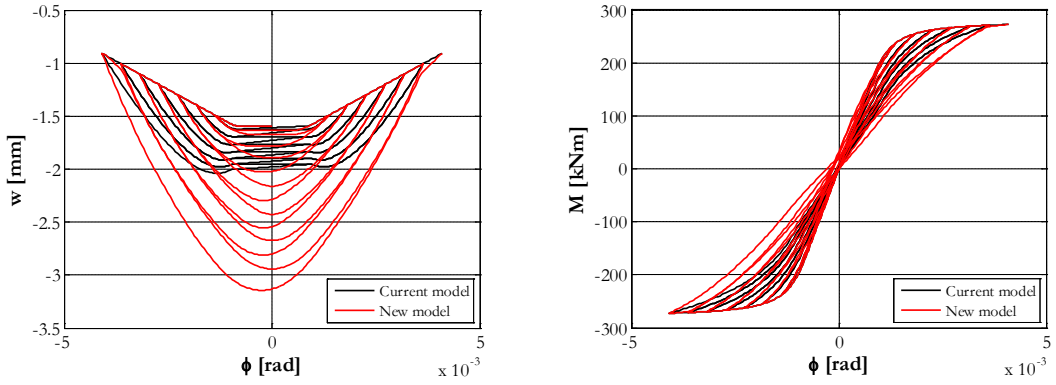

Fig. 6 – Comparison between the current (black lines) and improved (red lines) macroelement model, in terms of vertical displacement vs. rotation (left) and moment vs. rotation (right) at constant axial load

4. Validation of the improved macroelement model

In order to validate the improved macroelement model, an equivalent spring model was developed. Spring models have often been used to model macroelement sections with nonlinear behaviour (e.g. [16]): in this model the length of the interface corresponding to the lower part of the macroelement was discretized into a certain number of portions. The behaviour of each portion is represented by a nonlinear spring with the same

constitutive rule already used for the macroelement (Fig. 3 - right). At each load step the stress of each spring was determined according to the constitutive rule and the nonlinear *N* and *M* were calculated integrating the nonlinear stresses over the section. The advantage of the improved macroelement model with respect to the spring model is the reduced amount of variables on which the nonlinear behaviour depends. This allows a reduced computational burden, especially when applied to the analysis of buildings, characterized by a high number of elements. In order to validate the improved macroelement model, the behaviour of a calcium-silicate wall of length 2 m, height 2.2 m, thickness 0.1 m, material properties equal to the ones of the previous example and subjected to a constant vertical displacement (0.015 m downwards) and an increasing cyclic rotation up to a value of $4x10^{-3}$ rad was simulated by means of both the improved macroelement and the spring model. For the sake of simplicity, only the lower part of the macroelement (i.e. one single interface) was considered. As an example, Fig. 7 presents the axial load (left) and the moment (right) versus the imposed rotation, obtained by means of the spring model. When comparing the results obtained by means of the spring model to the ones obtained by means of the improved macroelement model, it can be noticed that no difference is evident, thus confirming the ability of the developed model of simulating the nonlinear behaviour.

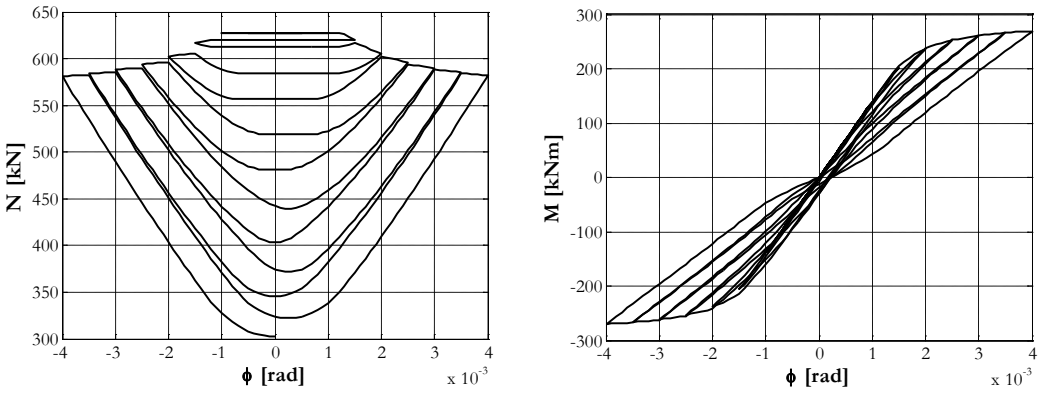

Fig. 7 – Axial load (left) and moment (right) vs. rotation obtained with the spring model

5. Simulation of experimental tests

In order to show the ability of the improved macroelement model to reproduce the experimental behaviour of masonry walls, the simulation of different experimental tests was performed. In particular, the improved macroelement was used to simulate in-plane quasi static cyclic tests performed on full-scale masonry piers.

5.1 ESECMaSE calcium-silicate in-plane tests

The first test campaign considered in the simulation work is the one performed at EUCENTRE in Pavia (Italy) in the framework of the project “Enhanced Safety and Efficient Construction of Masonry Structures in Europe” - ESECMaSE [18]. Walls made of blocks of different typologies were tested; however, in this simulation work only the tests on calcium-silicate walls were considered. Morevover, only test CS 05 was simulated since it was the only one showing a clear flexural failure. In particular, wall CS 05 remained undamaged with only some tension cracks in the joints up to a top displacement of 35 mm. When this displacement was exceeded, the specimen suddenly failed in shear with the development of a diagonal crack in the mortar bedjoints and in the units. Before this displacement, the force-displacement curves were characterized by S-shaped cycles with low energy dissipation, typical of a rocking behaviour. The left part of Fig. 8 shows the specimen at the end of the test, whereas the right part shows the comparison among the base shear vs. top displacement curves obtained from the experimental test and the numerical simulations by means of TREMURI, using the current and the new constitutive relationship. With respect to the current macroelement model, a significant increase of the dissipated energy is evident when using the new constitutive law.

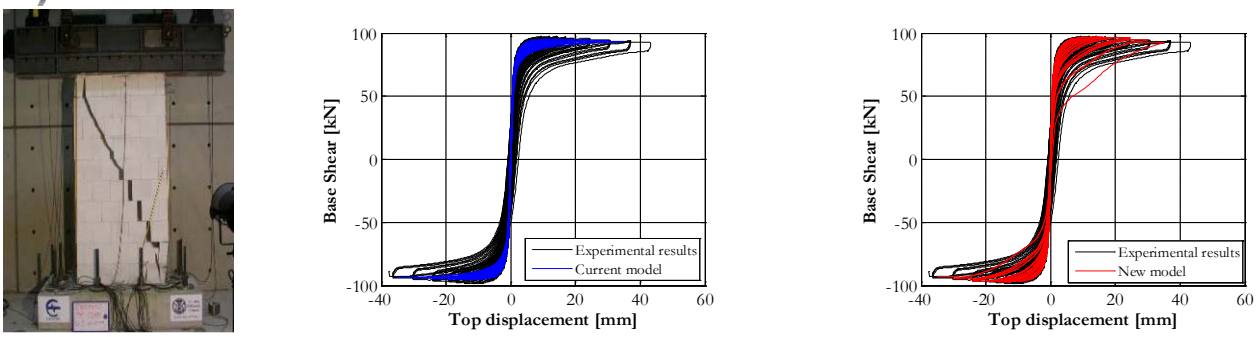

Fig. 8 – Specimen CS 05 at the end of the test (left) and comparison among the base shear vs. top displacement curves obtained from experimental test and numerical simulation with the current (centre) and the new (right) TREMURI constitutive model for wall CS 05

5.2 EUCENTRE calcium-silicate in-plane tests

The second experimental campaign considered in the simulation work is the one recently performed at EUCENTRE in Pavia (Italy) on calcium-silicate brick masonry [17]. The large experimental campaign included three in-plane quasi-static cyclic shear-compression tests on full scale calcium-silicate unreinforced masonry walls with different combinations of vertical compression, boundary conditions and slenderness ratios. Only specimen EC_COMP_1 and EC_COMP_2 have been considered in the simulation work, since these were the only walls showing a rocking behaviour. In particular, wall EC_COMP_1 was characterized by a rocking behaviour with cracks opening at the edges, without visible damage in the masonry panel. A migration of the horizontal cracks at the bottom was observed: in particular, these cracks were located at the interface up to a drift of 0.6%, above the first brick layer up to a drift of 1.5% and above the second brick layer during the last cycle with a drift of 2%. At the end of the test the failure mechanism was characterized by toe-crushing at the top and bottom of the wall with expulsion of brick and mortar. It should be noted that a pure rocking behaviour can be observed only in terms of cracking pattern and not in terms of hysteresis curve (Fig. 9). Specimen EC_COMP_2 showed a pure rocking behaviour with cracks opening at the edges, without visible damage in the masonry panel. It should be noticed that, due to the significant difference of in plane and out-of-plane slenderness of the wall, the reinforced concrete beam at the top of the specimen started to rotate after 0.15% drift. Consequently, the end of the test was reached for out-of-plane failure of the wall at a drift equal to 0.25%.

For specimens EC_COMP_1 and EC_COMP_2 the simulation was performed with three different sets of values of shear strength mechanical properties (i.e. cohesion c and friction coefficient μ), since it was evident that a single set of values was not sufficient to reproduce the experimental behaviour in all the cycles of the tests. Only the results using the set of parameters used to reproduce flexural behavior are considered in this paper, since they are the only ones affected by the flexural model.

Fig. 9 and Fig. 10 shows the specimen (left) and the comparison among the base shear vs. top displacement curves obtained from the experimental test and the numerical simulations by means of TREMURI using the current (centre) and the new (right) constitutive relationship for specimen EC_COMP_1 and EC_COMP_2 respectively. As regards wall EC_COMP_1, it can be noticed that, with the selected parameters, it is possible to capture the strength corresponding to the first plateau, although it is not possible to model the following increase of strength and the energy dissipation is underestimated. Furthermore, it is possible to notice an increment of the dissipated energy when using the new constitutive law with respect to the current one. On the contrary, in the case of wall EC_COMP_2, no difference between the new and the current constitutive law can be appreciated and the energy dissipation is significantly lower than the experimental one.

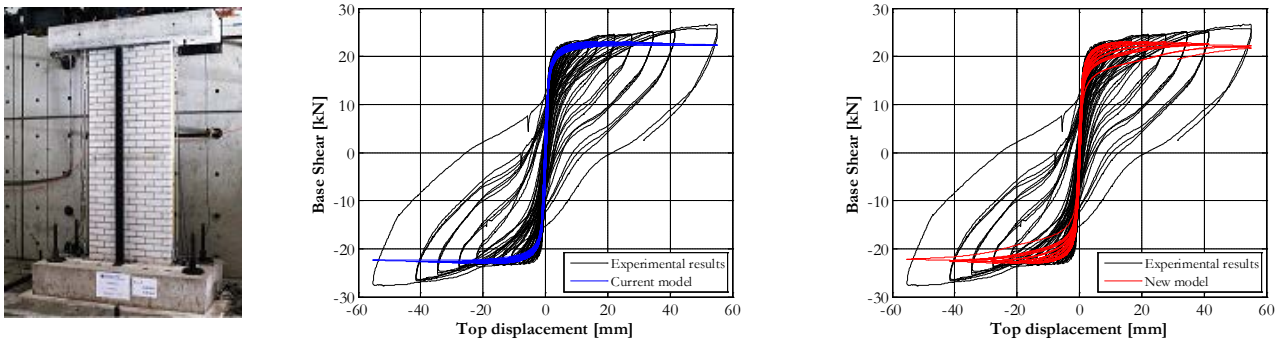

Fig. 9 – Wall EC_COMP_1: view of the specimen (left) and comparison among the base shear vs. top displacement curves obtained from experimental tests and numerical simulation with the current (centre) and the new (right) TREMURI constitutive model

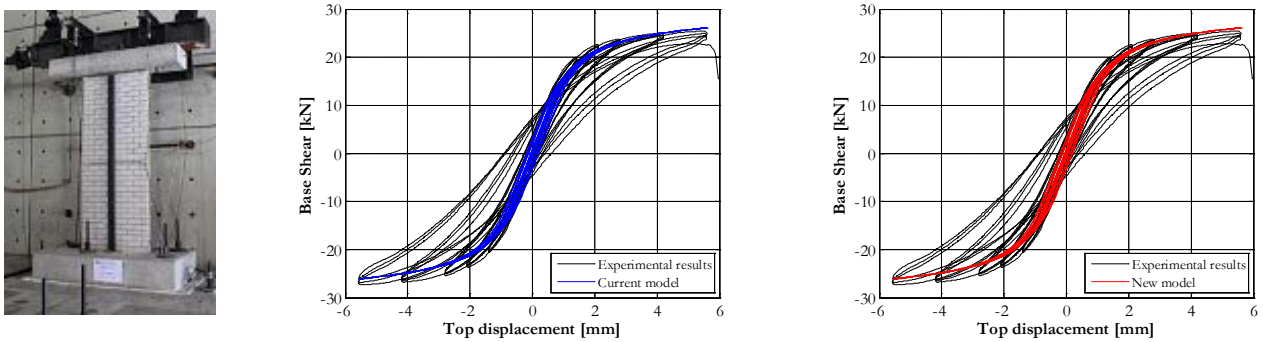

Fig. 10 – Wall EC_COMP_2: view of the specimen (left) and comparison among the base shear vs. top displacement curves obtained from experimental tests and numerical simulation with the current (centre) and the new (right) TREMURI constitutive model

A parametric study on the influence of the compressive strength on the dissipated energy predicted by the new constitutive model was performed with reference to wall EC_COMP_1. The value of compressive strength was progressively reduced starting from 6.3 MPa, i.e. the value used in the simulation of experimental tests (equal to the value obtained from the material characterization tests of the experimental campaign described in [17]): the sequence of values used is 6.3 MPa, 6.0 MPa, 5.8 MPa and 5.6 MPa. A further reduction of compressive strength was not possible since the results started to show meaningless behaviours, probably related to the failure of the whole section of the wall. The results of this parametric study are reported in Fig. 11.

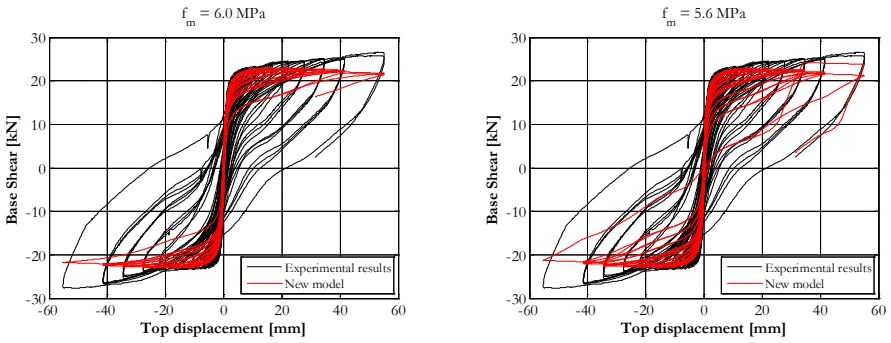

Fig. 11 – Comparison among the base shear vs. top displacement curves obtained from experimental tests and numerical simulation with the new TREMURI constitutive model for EC_COMP_1 wall, using different values of compressive strength

It can be noticed that, reducing the compressive strength, the energy dissipation significantly increases and the shear strength remains unchanged. In particular, the best prediction in terms of energy dissipation can be obtained with the lowest value of f_m, i.e. 5.6 MPa, although it was not still possible to capture the hysteretic behavior at the last cycles. In this case, it seems that, in order to better predict the energy dissipation, a value equal to the 90% of the nominal compressive strength needs to be used. This achievement needs to be checked extending this parametric study to other experimental tests.

6. Conclusions

In this work, a new constitutive law for flexural behaviour of masonry panels was proposed and implemented in the macroelement model proposed in [11], in order to better capture the energy dissipation observed in experimental tests on some masonry typologies, such as the calcium-silicate masonry. This law is characterized, as the one proposed in [11], by zero tensile strength and by an elasto-plastic behaviour in compression. Differently from [11], the unloading stiffness is now equal to the initial stiffness, thus having the possibility of modelling accumulation of displacement during a general loading history. The new constitutive law was then implemented in the software TREMURI [12] for the nonlinear analysis of masonry buildings. The new macroelement model was validated by comparing the results of a virtual test with the ones obtained using a spring model with the same constitutive law. Finally, the simulation of different experimental tests on calcium-silicate walls was performed with both the current and the new constitutive law.

This work allows to investigate the ability of the new model of capturing the energy dissipation observed in the experimental tests. The simulation indicated that the new law is actually predicting an increased energy dissipation with respect to the one of the macroelement model proposed in [11], but this is still quite low compared to the experimental one. Therefore, there is still an amount of energy dissipation which cannot be captured by numerical models, probably due the difficulty of obtaining a pure flexural behavior in the considered experimental tests. A parametric study on the influence of the value of compressive strength on the amount of dissipated energy showed that this difference could be possibly reduced using a certain percentage (e.g. 90%) of the nominal value of compressive strength.

Finally, the ability of the new developed constitutive law of modelling both the displacement accumulation under cyclic loads and the absence of tensile strength, makes the model suitable to model the behaviour of the soil. Future developments of this work could thus consist in developing a foundation macroelement able of reproducing the interaction of soil and masonry structure, as done for example in [19] with reference to soil-pile-structure interaction in the seismic design of bridges.

7. Acknowledgements

The authors would like to acknowledge the Nederlandse Aardolie Maatschappij BV and EUCENTRE for providing the experimental data used in this work.

8. References

[1] Alpa G, Monetto I (1994): Microstructural model for dry block masonry walls with in-plane loading. *Journal of the Mechanics and Physics of Solid*, **47** (7), 1159-1175.

[2] Lourenco PB, Rots JG, Blaauwendraad J (1998): Continuum model for masonry: parameter estimation and validation, *ASCE Journal of Structural Engineering*, **124** (6), 642–652.

[3] Calderini C, Lagomarsino S (2008): A continuum model for in-plane anisotropic inelastic behaviour of masonry. *ASCE Journal of Structural Engineering*, **134** (2), 209–220.

[4] Lemos JV (2007): Discrete element modeling of masonry structures. *International Journal of Architectural Heritage: Conservation, Analysis, and Restoration*, **1** (2), 190–213.

[5] Casolo S, Peña F (2007): Rigid element model for in-plane dynamics of masonry walls considering hysteretic behavior and damage. *Earthquake Engineering & Structural Dynamics*, **36** (8), 1029–1048.

[6] Tomaževič M (1987): Dynamic modelling of masonry buildings: storey mechanism model as a simple alternative. *Earthquake Engineering & Structural Dynamics*, **15** (6), 731–749.

[7] Milani G, Lourenço PB, Tralli A (2007): 3D homogenized limit analysis of masonry buildings under horizontal loads. *Engineering Structures*, **29**, 3134–3148.

[8] Magenes G, Braggio C, Bolognini D (2001): Metodi Semplificati per l'analisi Sismica non Lineare di Edifici in Muratura. *CNR-GNDT*, Rome, Italy (in Italian).

[9] Magenes G, Della Fontana A (1998): Simplified non-linear seismic analysis of masonry buildings. *Proceedings of the British Masonry Society*, **8**, 190-195.

[10] Belmouden Y, Lestuzzi P (2009): An equivalent frame model for seismic analysis of masonry and reinforced concrete buildings. *Construction and Building Materials*, **23** (1), 40–53.

[11] Penna A, Lagomarsino S, Galasco A (2014): A nonlinear macroelement model for the seismic analysis of masonry buildings. *Earthquake Engineering & Structural Dynamics*, **43** (2), 159-179.

[12] Lagomarsino S, Penna A, Galasco A, Cattari S (2013): TREMURI program: an equivalent frame model for the nonlinear seismic analysis of masonry buildings. *Engineering Structures*, **56** (11), 1787-1799.

[13] Abrams DP (1992): Strength and behaviour of unreinforced masonry elements. *10th World Conference on Earthquake Engineering*, Madrid, Spain.

[14] Anthoine A, Magonette G, Magenes G (1995): Shear-compression testing and analysis of brick masonry walls. *10th European Conference on Earthquake Engineering*, Vienna, Austria.

[15] Magenes G, Calvi GM (1997): In-plane seismic response of brick masonry walls. *Earthquake Engineering & Structural Dynamics*, **26**, 1091-1112.

[16] Abbas N (2013): Non-linear soil-structure interaction: formulation of a macro-element and application to non-linear static and dynamic analyses of masonry structures. *PhD Thesis*, University of Genoa, Italy.

[17] Graziotti F, Rossi A, Mandirola M, Penna A, Magenes G (2016): Experimental characterization of calcium-silicate brick masonry for seismic assessment. *16th International Brick and Block Masonry Conference*, Padova, Italy.

[18] Magenes G, Morandi P, Penna A (2008): Test results on the behaviour of masonry under static cyclic in plane lateral loads. *Technical Report D 7.1c*, EUCENTRE, Pavia, Italy.

[19] Correia AA (2011): Soil-pile structure interaction in seismic design of bridges: towards macro-element modelling for performance-based earthquake engineering. *PhD Thesis*, European School for Advanced Studies in Reduction of Seismic Risk (ROSE School), University of Pavia, Italy.